EUROPEAN ORGANIZATION FOR NUCLEAR RESEARCH
European Laboratory for Particle Physics

Dipatimento IA di Fisica dell'Università and INFN

Bari
Italy

Internal Note/

ALICE reference number
ALICE-INT-2005-011 version 1.0
Institute reference number
[-]
Date of last change
2005-04-26

Sensor thickness dependence of the ALICE Silicon Pixel Detector performance

Authors:

G.E. Bruno, M. Caselle, D. Elia[1], V. Manzari, F. Navach, R. Santoro
Dipartimento IA di Fisica dell'Università and INFN, Bari (Italy)

Abstract:

Prototypes of the ALICE Silicon Pixel Detector with 200 and 300 μm thick sensors have been tested in beam at SPS in two similar measurements performed in 2002 and 2003 respectively. We compare in this note results obtained for the two detector configurations.

[1]Corresponding author, e-mail: Domenico.Elia@ba.infn.it

1 Introduction

Prototypes of the ALICE Silicon Pixel Detector (SPD) have been exposed in 2002 and 2003 to proton beams at the SPS. The experimental setup (Fig.1) consisted of a tracking system made by four pixel planes arranged in two doublets (*minibus* configuration). Data was taken with several global threshold settings on the detector and for various incidence angles of the beam. A complete study of the main detector performances, such as spatial precision and efficiency, has been reported previuosly [1] for a 300 μm thick sensor. In its final configuration the ALICE SPD has a 200 μm thick sensor substrate [2]. In this note, we report on a comparison of the performances obtained with the thin (200 μm) and thick (300 μm) versions of the prototype.

2 Beam test with the thin prototype

This beam test has been carried out in the North Hall at CERN in July 2002. Detectors were placed at the SPS H4 line and irradiated with a 350 GeV/c proton beam [3, 4]. All the tracking detectors in the doublets were placed with the shortest (50 μm) pixel cell side along the y coordinate, conversely with the test for the thick prototype where a crossed geometry was adopted [1, 5]. This allows very precise studies in the y coordinate where also the test detector had the shortest cell size direction.
The detector under test was a prototype of the ALICE SPD made by an assembly of a 200 μm thick sensor and 750 μm thick ALICE1 front-end chip [6]. The two minibus doublets were made by assemblies of the same front-end chip and 300 μm thick sensor. The transverse position and the tilt angle of the test plane with respect to the beam axis could be changed by a remote controlled stepping motor. The trigger signal was derived from the signal delivered by scintillator counters upon the passage of beam particles.
Data was collected with different beam incidence angles obtained by a rotation of the test detector along an axis parallel to the 425 μm long cell side direction (x coordinate). An angle scan (from 0 to 30, in steps of 5 degrees) was performed for three different values of the global threshold, around the typical operating setting.
For the configuration with normal incidence beam a full scan of the global threshold setting on the detector has been performed, namely in DAC units from 210 (corresponding to about 2500 electrons) down to 60. Each 15 units decrease in the DAC value corresponds to about 1000 electrons increase in the effective global threshold: this linearity holds for DAC values above 150. For details on the measurement of mean threshold and mean noise as a function of the global threshold setting on the chip see [7].

3 Data analysis and results

Data samples from both tests with the thin and the thick detectors have been analyzed in the same way. As a preliminary step, the hits on the detector planes are processed by a cluster finder algorithm: a cluster is by definition either a single fired pixel or a group of fired pixels, each of them being adjacent to at least another one. For each event and each plane, the cluster finder analysis works out the number of clusters and, for each cluster, the number of hit pixels (cluster size), the x and y dimensions and the topology. Fig.2 illustrates the cluster topology numbering conventionally used.

Before starting the track reconstruction procedure, the relative misalignments of the detectors in the transverse directions has to be taken into account. Details on this alignment method are reported in [1]. After plane alignment, the beam track is reconstructed with a best fit method through the space points registered by the minibus doublets. Specific features coming from differences in the experimental setup of the tracking doublets used for the test of the thin and thick detector are discussed next.

Events in which the beam passes through the sensitive area of the detector under test are selected. Clusters on the test plane are then tagged as correlated with the beam track when the difference (residual) between the track prediction from the telescope and the mean cluster position[1] fulfils the following conditions: $\Delta x < 750$ μm and $\Delta y < 150$ μm. This choice is based on the observed number of selected clusters as a function of the applied distance cut and corresponds to $\approx 10\sigma$ of the measured residual distributions.

The estimate of the precision in the track impact prediction on the test plane, as provided by the telescope, has been done with the same procedure used for 2003 data: it is based on a simulation taking into account the telescope geometry, multiple scattering and residual plane misalignments effects (for details see [1]). In the x coordinate direction the precision is much worse than for the thick detector test, due to the different minibus configuration. It is however better in the y coordinate: we have estimated $\sigma_{track}(y) \approx 6$ μm, to be compared with a value of ≈ 10 μm found for setup of the thick detector test (see Fig.3). The contribution to these precisions coming from the multiple scattering has been found negligible in both configurations [1, 8].

As a first comparison, the frequency of each cluster topology at 200 DAC units threshold for thick (top) and thin sensors (bottom) is shown in Fig.4: only tagged clusters are taken into account. The fractions of single and double-y pixel clusters for the thin sensor detector correspond to 68% and 27% respectively, while they were found to be 58% and 35% for the 300 μm thick sensors case [1].

[1]The measured cluster position is taken as the mean of the center positions of all the hit pixels in the cluster.

Fig.5 shows the total residual distributions for both sensor thicknesses, in the y coordinate (along the 50 μm pixel size). The widths of the residual distributions in the two cases are different, but the different tracking precisions have also to be taken into account to extract the corresponding intrinsic spatial precisions [1, 8]. After subtracting the uncertainty on the telescope extrapolation, we find $\sigma^{200}_{pixel}(y) = (\ 11.1\ \pm\ 0.2\ )\ \mu m$, which compares with $\sigma^{300}_{pixel}(y) = (\ 11.0\ \pm\ 0.5\ )\ \mu m$ for the 300 μm sensor: the estimated global precisions (i.e. considering contributions from all cluster topologies) are thus equal for both sensor thicknesses at 200 DAC units threshold. The errors on the estimates of the intrinsic precision have been calculated by taking into account both the contributions due to uncertainties in the widths of the residual distributions and uncertainty in the tracking precision.
To better understand the behaviour of the two sensors, comparisons at 200 DAC units threshold have been done also separately for the main cluster topologies, i.e. single (cls 1) and double-y (cls 2) pixel clusters. For the 200 μm sensor we find:

$$\sigma^{cls1}_{pixel}(y) = (\ 11.5\ \pm\ 0.2\ )\ \mu m \qquad \sigma^{cls2}_{pixel}(y) = (\ 6.8\ \pm\ 0.3\ )\ \mu m \tag{1}$$

to be compared with the same quantities extracted for the thicker detector [1]:

$$\sigma^{cls1}_{pixel}(x) = (\ 11.0 \pm 0.5\ )\ \mu m \qquad \sigma^{cls2}_{pixel}(y) = (\ 9.2 \pm 0.6\ )\ \mu m \quad . \tag{2}$$

We see that, with the same threshold setting, the thin detector provides a better double pixel cluster precision than the 300 μm one. As expected, to generate a double pixel cluster tracks have to traverse the detector in a region (around the boundary between the two adjacent pixels) which is narrower for the thin detector than for the thick one. In the next subsection, the corresponding evolutions obtained by varying the threshold setting will show in more detail the differences between the two detectors.

3.1 Study of global threshold scan

For normal beam incidence, the studies performed as a function of the threshold setting for the 300 μm sensor have been repeated carried out for the thin sensor. In Fig.6 and Fig.7 we show the cluster size distributions at different threshold values, for the thick and the thin sensor respectively. Also scatter plots of the dimensions in x ($dimx$) and y ($dimy$) coordinates of the corresponding boundary boxes (minimal area boxes containing the cluster) are illustrated.
We observe that even at the lowest threshold setting corresponding to 210 DAC, for the

thin sensor the single pixel clusters are still more frequent than the double pixel ones. We thus expect that the absolute minimum in the intrinsic precision as a function of the threshold, as seen for thick sensor, cannot be reached for the 200 μm sensor. The comparison of the average cluster size as a function of a decreasing threshold setting is shown in Fig.8. Details on the evolution of cluster topology distributions have also been studied, like for the thick sensor data. All these comparisons and those coming from the track incidence angle scan study are found very useful for the tuning of the detector response in the SPD simulation [9].

The spatial precision of the detector has been studied also as a function of the threshold: results are illustrated in Fig.9. The comparison between the two sensors indicates a steeper dependence on the threshold for the thin detector than for the thick one. Smooth curves resulting from a spline approximation algorithm have been superimposed. The two curves corresponding to the thick and thin detector cross each other at 200 DAC units threshold (as anticipated above) and again at 150 DAC units. At the lowest threshold setting corresponding to 210 DAC units the 200 μm sensor shows a better precision than the thick one. This can be interpreted as the result of a reduced diffusion process (drifting of the hole/electron clouds): this reduction can improve the minimum achievable precision under the condition that a proper threshold setting allows to have similar fractions of single and double-y pixel clusters. The absolute minimum precision for the thinner sensor is not even reached at 210 DAC units since still not perferct balancing of cluster topologies 1 and 3 is reached for that threshold setting.

The thin detector precision curve reaches a maximum around 150-160 DAC setting, with a corresponding value approaching $L_y/\sqrt{12}$ ($L_y = 50$ μm being the pixel cell size along the y direction). Tracks impacting a cell too close to the boundary regions share the produced charge almost equally in two adjacent pixels: for very high thresholds (DAC values smaller than 160 for the 200 μm sensor case) it can happen that none of the two pixels are fired, hence the sensitive region of the pixel cell gets effectively reduced. This explains the decrease of the intrinsic precision curve which appears at the same threshold setting where the efficiency also starts to decrease with respect to the plateau value, as will be shown in the following. Due to the larger amount of charge available, this feature is not observed (Fig.9) for the 300 μm sensor detector where the maximum appears for DAC values much lower than 150[2]. Fig.10 shows the intrinsic precisions separately for the two cluster topologies: the crossing point occurring at 210 DAC setting for the 300 μm sensor is not yet reached in the 200 μm one case.

[2]The DAC setting at which precision curves have the maximum corresponds to an affective global threshold in electrons close to half of the expected released charge in each of the two sensors.

In Fig.11 we show the comparison of the detection efficiencies as a function of the threshold setting. The efficiencies for both detectors reach a plateau at 99% and, as expected, the efficiency for the thin detector is lower than for the thick detector at low threshold values. Therefore, the plateau value is reached at higher threshold values in the case of thin detector than in the case of thick one. As anticipated above, the efficiency for the 200 μm sensor detector starts to decrease at DAC settings below 150 units. The superimposed curves are the result of the fit to the gaussian-integral function: the good agreement with the data is an hint for a linear behaviour of the DAC setting with the threshold in a wide range of values.

3.2 Study of track inclination angle scan

The dependence of the detector performance as a function of the beam incidence angle has been studied also for the thin sensor detector. As already mentioned, data samples at 0, 5, 10, 15, 20, 25 and 30 degrees incidence angles were taken with thresholds set at 185, 200 and 210 DAC units.

Fig.12 schematically shows pixel cells traversed by a track at three different incidence angles, where both the cases of 300 and 200 μm sensor thicknesses are compared. The geometry basically explains the evolution of the average cluster sizes as a function of the track incidence at the different threshold settings (Fig.13). The behaviour seen for the 300 μm sensor detector at very large inclination angles and high thresholds [1] could not be observed for the thin sensor case where data foe angles above 30 degrees is not available. Fig.14 shows the evolution in the cluster topology by varying the track incidence angle.

The results of the study on the spatial precision as a function of the track incidence angles are shown in Fig.15. Due to the different evolution of the cluster topology for the two sensor thicknesses, we see also a different pattern in the corresponding precision behaviours. For instance, the curves at 185 and 200 DAC setting reach the minimum for 10 degrees incidence angle tracks: this is just because for that value of the angle, as already seen, the fraction of single and double pixel clusters are rougthly equal. For the lower threshold of 210 DAC units, the optimal precision occurs at a slightly smaller angle, again where a balance of the two main pixel cluster topology frequencies occurs. The precision also degrades for all the threshold settings with the increasing track angle, as expected when higher cluster topologies are involved. The pattern for the thicker sensor is quite different: the worst value for 10 degrees track angle can be explained with the particular geometry for this sensor. As seen in [1], for that angle the optimal precision occurs around 160 DAC which is far from the region of interest: at threshold values above 160 the double pixel clusters dominate over the single pixel ones with a degradation of

the corresponding intrinsic precision.
In Fig.16 the intrinsic precisions for the 200 μm sensor are shown together with the contributions due to the main pixel cluster topologies (namely topologies 1, 2 and 3), again as a function of the track inclination angle and for the 185, 200 and 210 DAC threshold settings. As in other plots, smooth curves from spline are meant to guide the eye; the estimated error on each point is also shown. Those measurements can be particularly useful in the tuning of the tracking errors to be associated to the SPD clusters, both in the simulation and in the real data analysis.

4 Summary

The ALICE Silicon Pixel Detector performance have been studied by using data collected in the 2002 and 2003 beam tests at the SPS. Data from the test of the 200 μm thick sensor detector, as in the final SPD configuration, has been fully analyzed: results on intrinsic spatial precision and detection efficiency have been compared with those corresponding to the 300 μm sensor used in 2003 test and previously studied.
A rather complete picture of the detector behaviour as a function of the threshold setting and track inclination angle is presented. The comparison between the two sensor thicknesses shows, in particular, that the intrinsic precision for the thinner detector has a steeper variation with the threshold. For inclination angles below $\approx$ 15 degrees it has been found to be better than for the 300 μm sensor detector.

References

[1] D. Elia *et al.*, ALICE Internal Note, ALICE-INT-2005-007.

[2] ITS Technical Design Report, CERN/LHCC 99-12, 1999.

[3] P. Riedler *et al.*, Proceedings of the $PIXEL2002$ Workshop, Carmel (USA), published in the SLAC Electronics Conference archive.

[4] P. Riedler *et al.*, Proceedings of the $VERTEX2003$ Workshop, Lake Windermere, 2004, to be published on NIM A.

[5] P. Nilsson *et al.*, Proceedings of the 10^{th} Vienna Conference on Instrumentation, Vienna (Austria), February 2004, to be published on NIM A.

[6] R. Dinapoli *et al.*, Proceedings of the 6^{th} Workshop on Electronics for LHC Experiments, Krakow (Poland), September 2000, CERN-2000-010.

[7] P. Riedler *et al.*, Proceedings of the 10^{th} International Workshop on Vertex Detectors, Brunnen (Switzerland), September 2001, Nucl. Instrum. Methods Phys. Res. A501 (2003), 111-118.

[8] J. Conrad and P. Nilsson, ALICE Internal Note, ALICE-INT-2005-003.

[9] G.E. Bruno *et al.*, *"A comparison of test beam data with the SPD simulations in AliRoot"*, in preparation as an ALICE Internal Note.

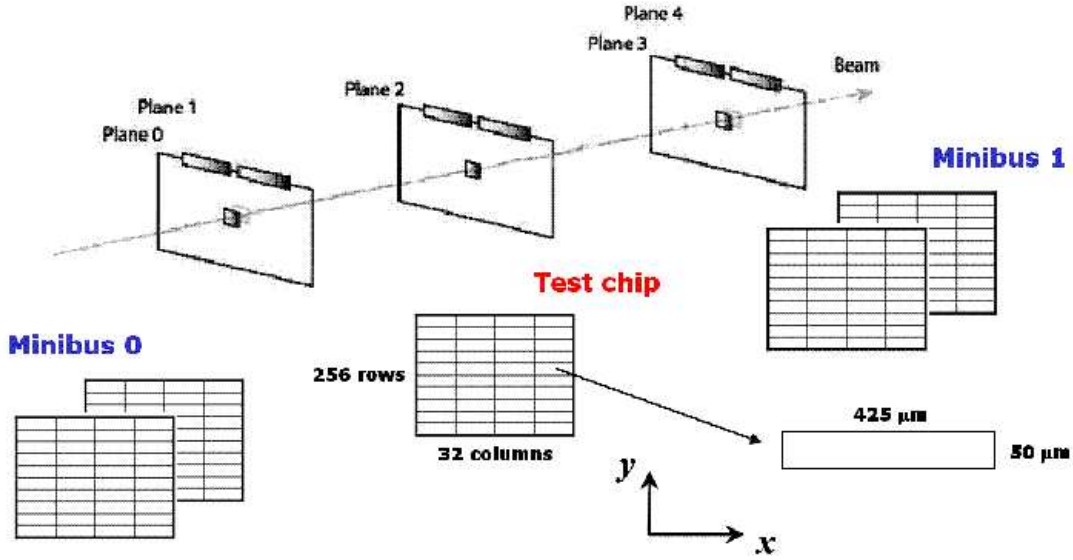

Figure 1: Schematic view of the layout for the 2002 beam test.

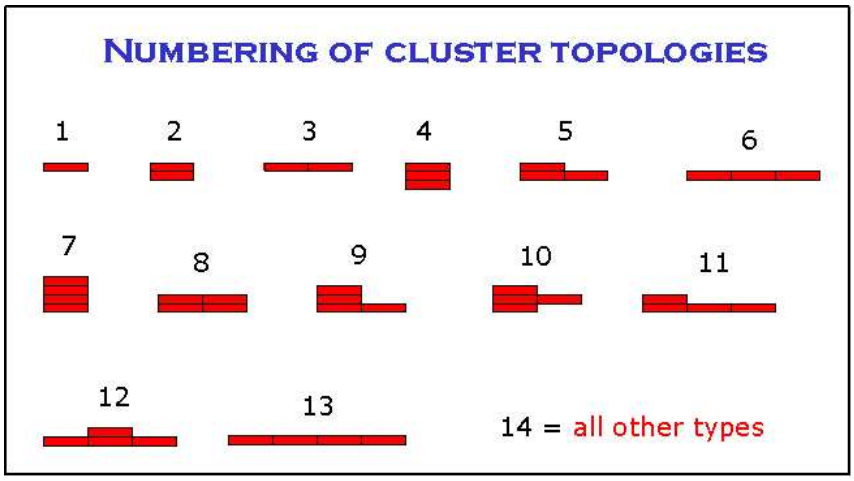

Figure 2: Numbering of the main pixel cluster topologies.

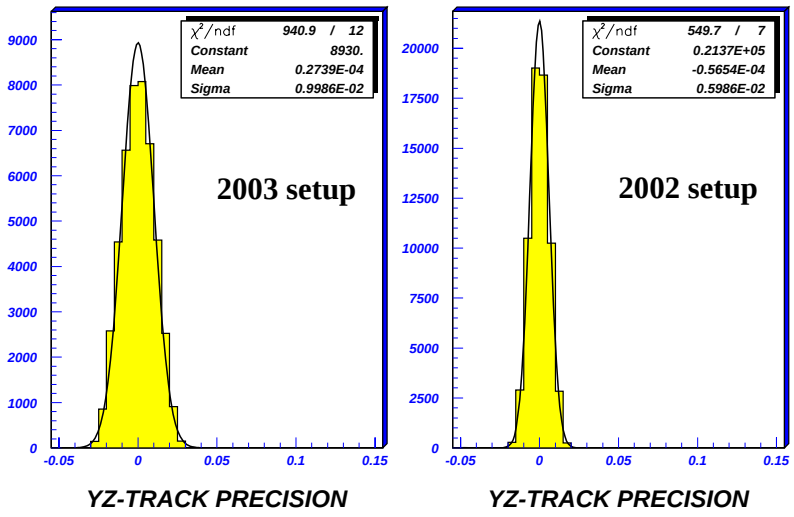

Figure 3: Difference in the y coordinate between predicted impacts and track crossing point from geometrical simulation, both for the 2003 (left) and 2002 (right) telescope configurations.

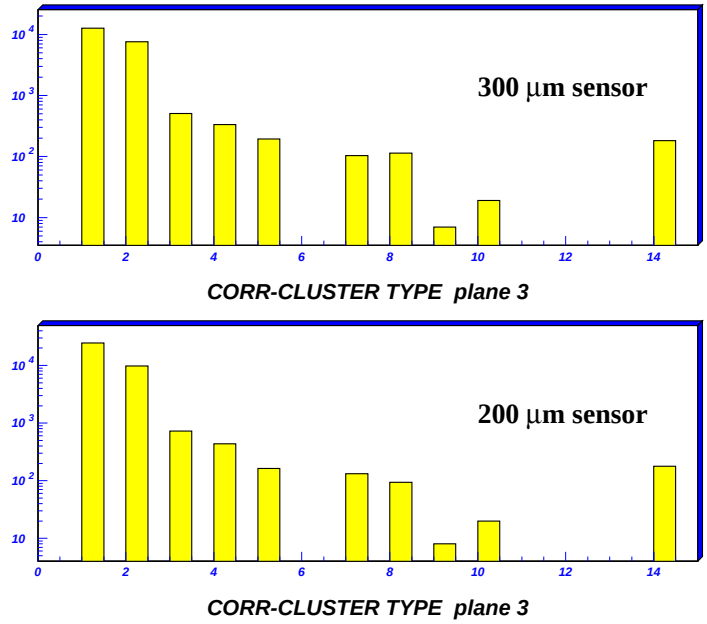

Figure 4: Distribution of cluster topologies on the test plane, for normal incidence tracks and threshold setting 200 DAC units, for the thick (top) and the thin (bottom) sensor cases.

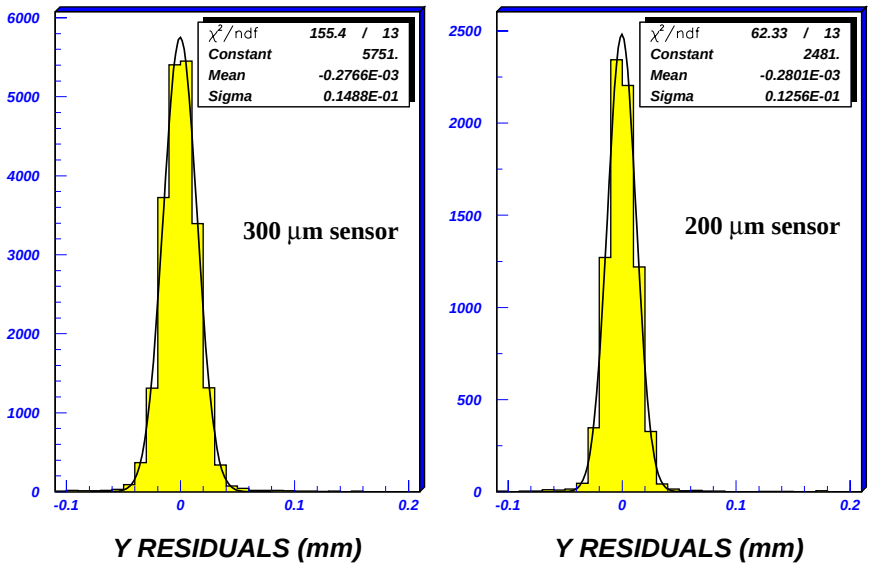

Figure 5: Residuals between predicted impact from the telescope and that from clusters on the test plane, for thick (left) and the thin (right) sensor detectors.

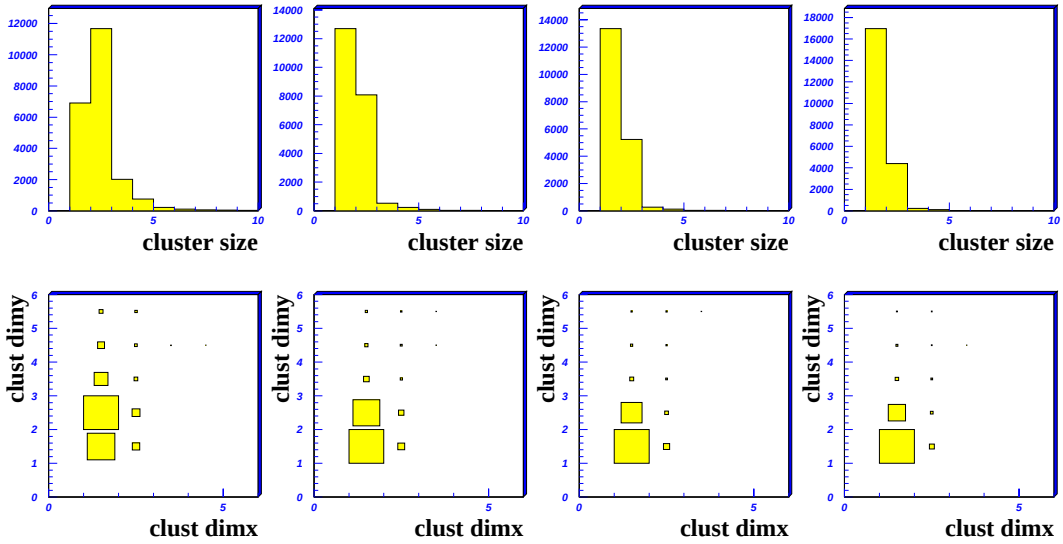

Figure 6: Cluster size distributions for the 300 μm sensor: from left to right threshold settings correspond to 214, 200, 180 and 160 DAC units.

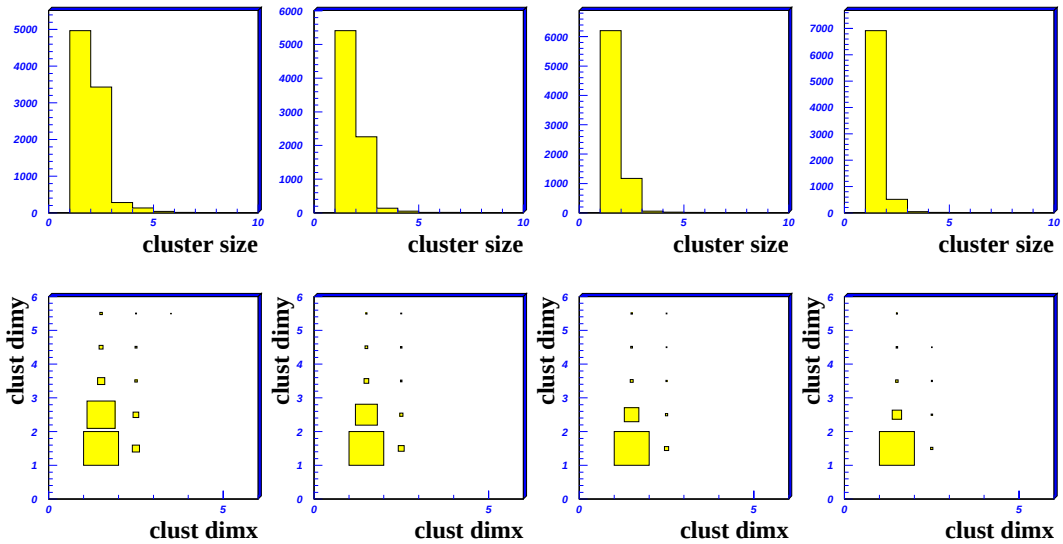

Figure 7: Cluster distributions for the 200 μm sensor: from left to right threshold settings correspond to 210, 200, 180 and 160 DAC units.

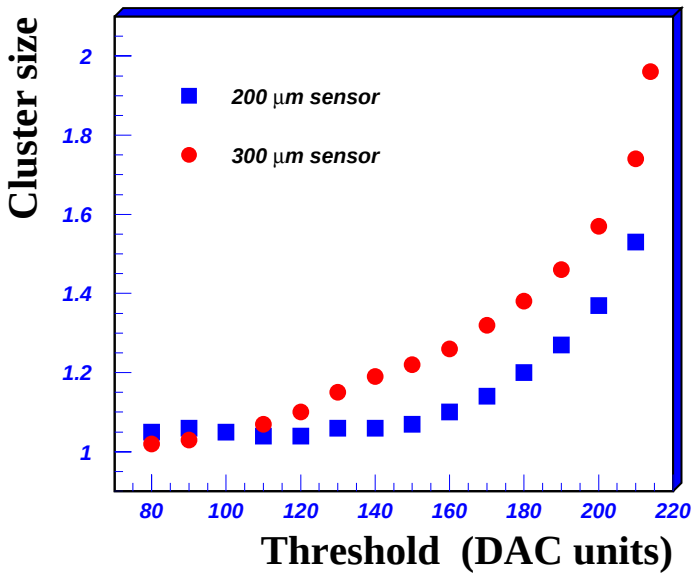

Figure 8: Average cluster size as a function of the threshold setting with normal track incidence angle and for both sensor thicknesses.

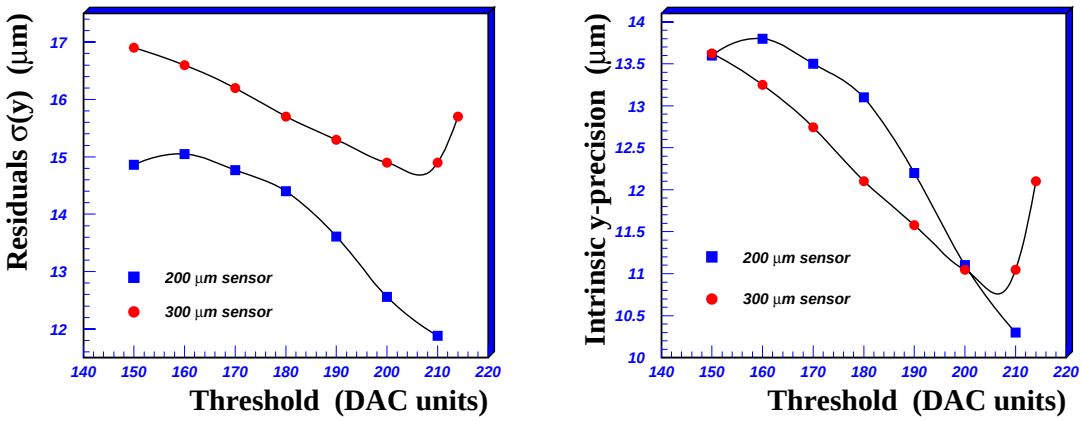

Figure 9: Width of the residual distribution along y coordinate as a function of the threshold (left) and corresponding intrinsic precision after subtraction of the telescope prediction uncertainties (right), for normal track incident angle samples and for both sensor thicknesses.

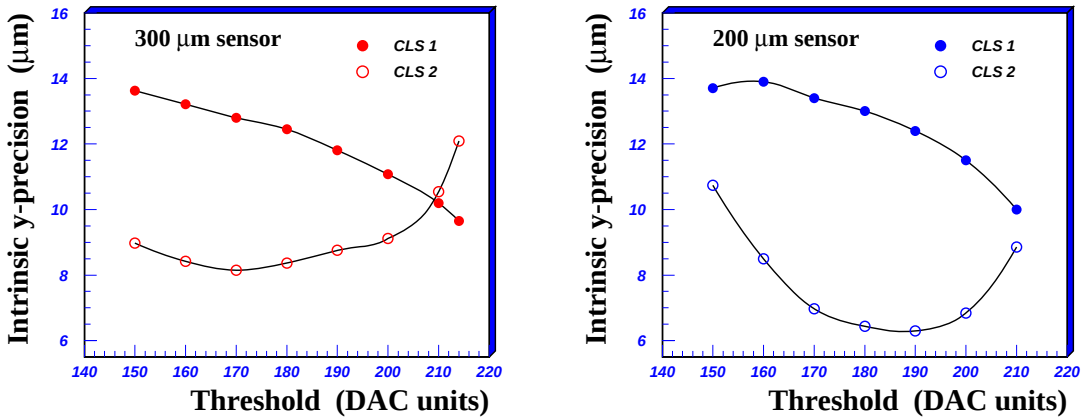

Figure 10: Intrinsic precision along the y coordinate for normal track incident angle samples as a function of the threshold and separately for cluster topology 1 (cls 1) and 3 (cls 2), for thick (left) and thin (right) sensor.

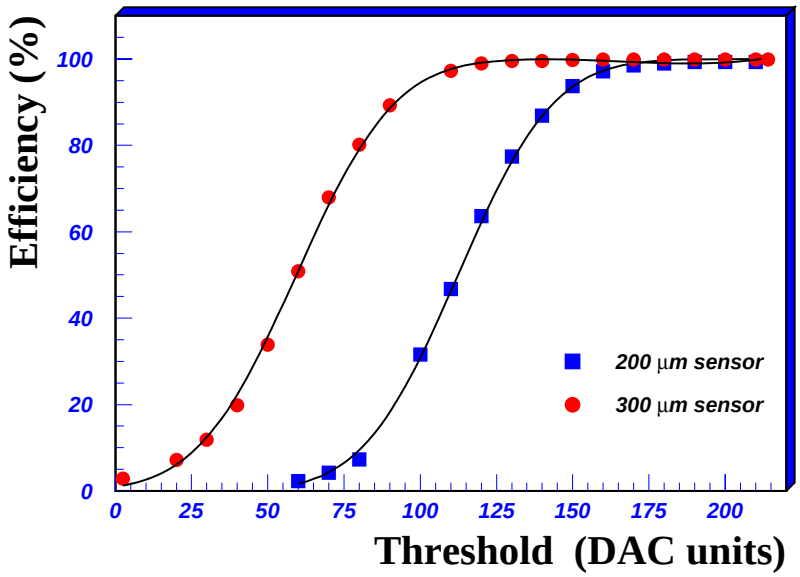

Figure 11: Detection efficiency as a function of the threshold for normal track incidence angle, for both sensor thicknesses. The results of a fit with gaussian-integral function are superimposed.

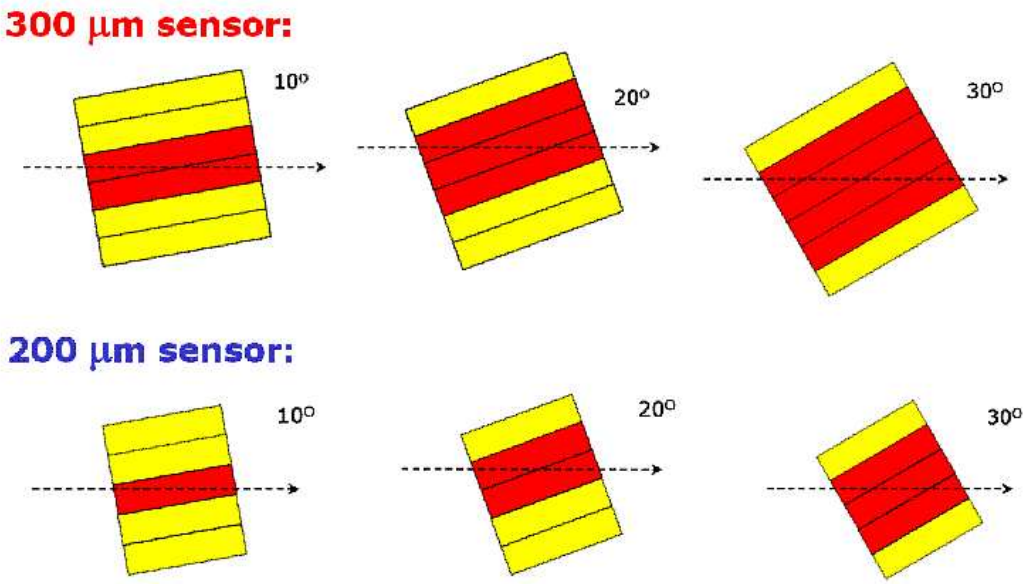

Figure 12: Schematic pictures of pixel planes crossed by tracks at different angles in the yz plane, for both sensor thicknesses. Pixel cells traversed by the track are shown in red.

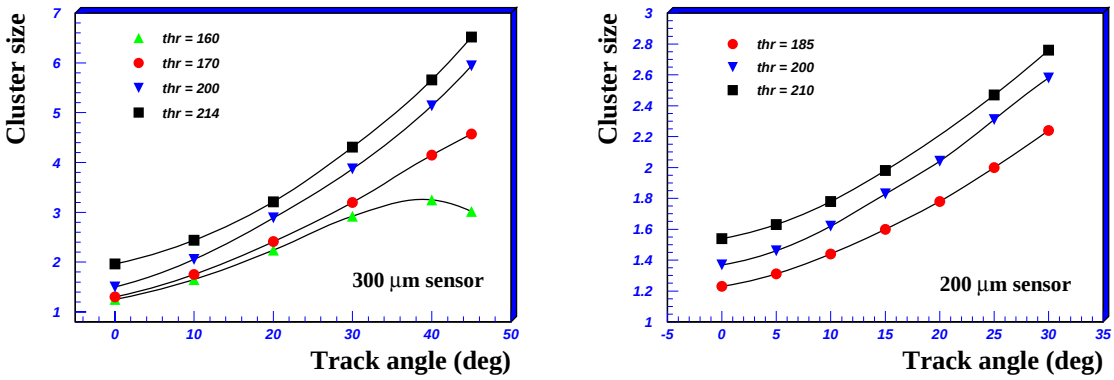

Figure 13: Average cluster size as a function of the track incidence angle at different thresholds settings, for thick (left) and thin (right) sensors.

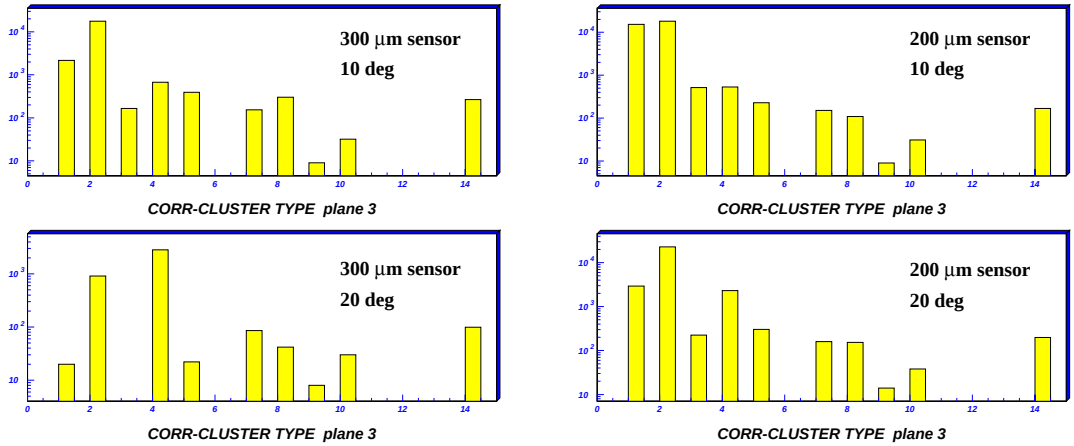

Figure 14: Cluster topology distributions for threshold settings of 200 DAC units, at 10 (top) and 20 degrees (bottom) track incidence angles. Thick and thin detector correspond to left and right hand side panels respectively.

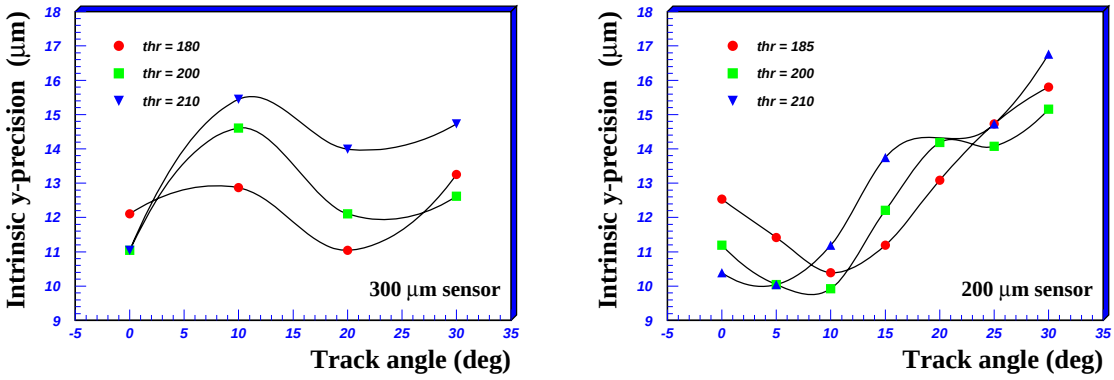

Figure 15: Intrinsic precision in the y coordinate as a function of the track incidence angle on the detector, at different threshold settings. Left and right hand side plots correspond to the 300 and 200 μm sensors respectively.

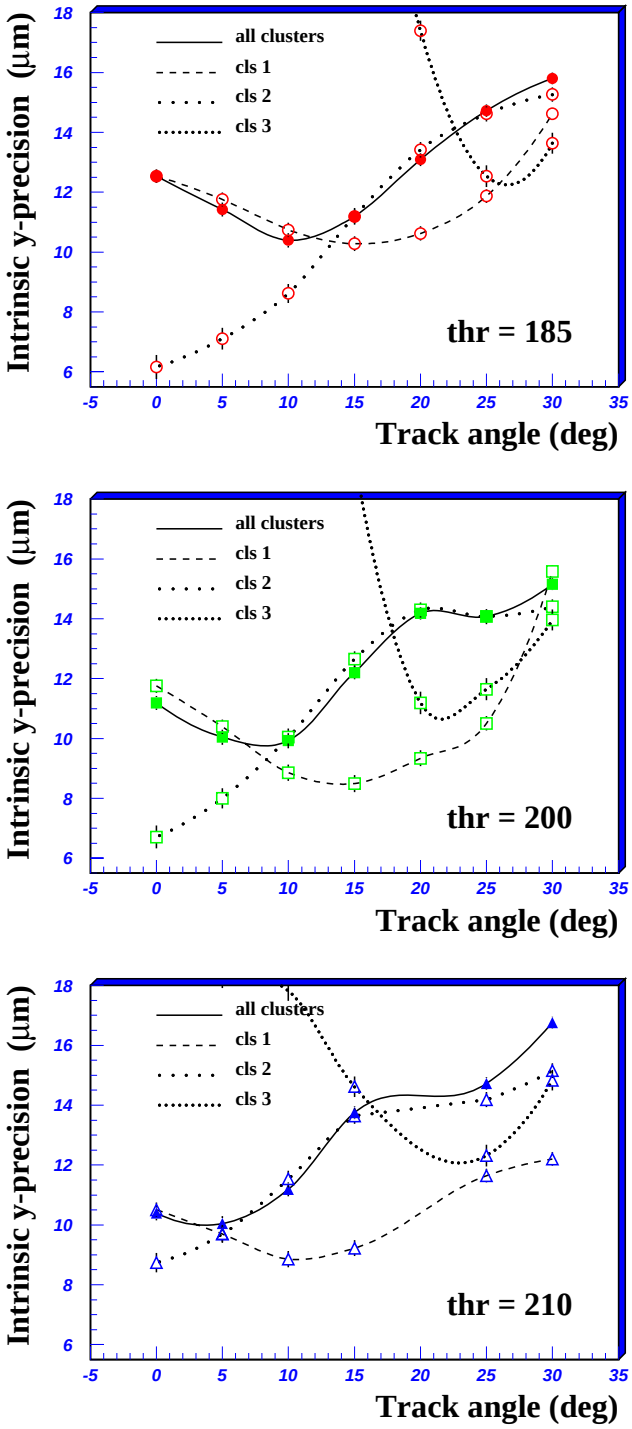

Figure 16: Intrinsic precision in the y coordinate as a function of the track incidence angle on the detector, for the 200 μm sensor. From top to bottom, the plots correspond to threshold settings of 185, 200 and 210 DAC: contribution to the global precision from different cluster topologies are shown.